Work Energy Relative Pressure Gradients using 2D Synthetic Aperture Ultrasound

Haslund, Lars Emil; Traberg, Marie Sand; Jensen, Jørgen Arendt

Published in:
Proceedings of 2023 IEEE International Ultrasonics Symposium

Link to article, DOI:
10.1109/IUS51837.2023.10307458

Publication date:
2023

Document Version
Peer reviewed version

Work Energy Relative Pressure Gradients using 2D Synthetic Aperture Ultrasound

Lars Emil Haslund, Marie Sand Traberg,
Jørgen Arendt Jensen, *IEEE Fellow*

Center for Fast Ultrasound Imaging, Department of Health Technology,
Technical University of Denmark, DK-2800 Lyngby, Denmark

***Abstract*—Pressure gradient estimations are used as a biomarker for cardiovascular diseases. Here non-invasive pressure gradients are desired over invasive catheterization. This study estimates non-invasive pressure gradients from synthetic aperture ultrasound using the work-energy method. The method is translated to 2D synthetic aperture ultrasound by assuming rotational symmetric blood vessels and is hypothesised to yield more precise estimation compared to the unsteady Bernoulli method along a streamline. The method uses flow rates, blood velocities and acceleration for estimating the pressure gradient. Data are acquired using a 256 elements, 6.5 MHz GE L3-12-D linear array transducer connected to a Verasonics research scanner with a pulse repetition frequency equal to 5 kHz. A interleaved sequence using 12 virtual sources is used for both flow estimations and B-mode imaging. The interleaved sequence allows correlation frames to be separated by only the pulse repetition time, making it possible to estimate high velocities. The work energy method is compared to a previously validated unsteady Bernoulli method (streamline method) using experimental data from a blood vessel phantom with a 60% stenosis. The result shows that the work-energy method detects a maximum pressure difference of 3.42 Pa and a minimum pressure difference of -53.3 Pa with a precision of 3.04% across eleven pulse cycles. The unsteady Bernoulli method detected pressure differences changing from 5.44 Pa to -68.2 Pa with a precision of 3.23%.**

I. Introduction

High pressure gradients across vascular compartment are used as biomarkers for cardiovascular diseases [1]. Current invasive procedures rely on fluid filled catheters or pressure wires and require an operation theater. These invasive techniques are evolving from being routine procedures to becoming much more specialized procedures, which are only applied when non-invasive methods have failed to diagnose the patient [2]. Non-invasive pressure gradients have been obtained using Doppler ultrasound [3] [4], and cardiac pressure gradients [5] [6] [7] have been acquired using color M-mode Doppler data. These techniques rely on clinical available imaging but are limited by the angle-dependent Doppler-derived velocities. To overcome this, different techniques have been used. Olesen et al. [8] used directional synthetic aperture ultrasound (SAU) for flow imaging [9] and for estimating the pressure differences. SAU was originally introduced by O'Donnell and L. J. Thomas for intravascular ultrasound imaging [10] and enables angle-independent blood velocity estimations [11] [12]. Magnetic Resonance Imaging (MRI) is also used for non-invasive pressure gradient estimations. Magnetic Resonance Imaging is a 4D modality [13] and are unlike ultrasound not limited by an acquisition window. MRI flow data have been used for the numerically modeling of cardiovascular pressure gradients [14] and to determine the pressure field across a diseased valve [15]. In 2015 Donati et al. [16] presented a work-energy approach for deriving pressure differences. Further development led to a virtual work-energy model [17], which has been applied to turbulent-driven flow fields [18] and intracardiac flow [19].

The purpose of this paper is to derive pressure differences from SAU data using the work energy approach and compare it to the unsteady Bernoulli method [20]. The work-energy method is based on cross-sectional velocity profiles, which are hypothesized to yield more robust estimates compared to the unsteady Bernoulli method, which is sensitive to local flow disturbances along a streamline. Both are intended for applications in the carotid arteries, which is a typical site for atherosclerosis [21].

II. Theory

This section describes the implemented work energy method presented in [22]. It is derived from the Navier-Stokes equation [16] and takes the following form:

$$\Delta P = -\frac{1}{Q}\left(\frac{\partial K_e}{\partial t} + A_e\right) \quad . \tag{1}$$

Here, ΔP, is the pressure difference between the outlet and the inlet, which are user selected. I.e., the user selects two cross-sections that constitute the inlet and the outlet. The flow rate Q, is measured in m^3/s and is given by:

$$Q = \int_{\alpha,\,outlet} \vec{v}\cdot\vec{n}\,dS = -\int_{\alpha,\,inlet} \vec{v}\cdot\vec{n}\,dS \quad . \tag{2}$$

Here, $\vec{n}$ denotes the normal direction of the inlet and outlet plane denoted by α. $dS = dz\cdot dy$, where dz and dy describe the sampling interval in the z- and y-direction. The kinetic energy, K_e, is measured in $Pa\cdot m^3$ and is given by:

$$K_e = \frac{\rho}{2}\int_{\Omega} \vec{v}\cdot\vec{v}\,dV \quad , \tag{3}$$

where Ω denotes the volume spanned by the inlet and the outlet, with $dV = dx\cdot dy\cdot dz$.

The advective energy A_e, is measured in $Pa \cdot m^3/s$ and is given by:

$$A_e = \frac{\rho}{2}\left(\int_{\alpha,inlet} |\vec{v}|^2 (\vec{v}\cdot\vec{n})\, dS + \int_{\alpha,outlet} |\vec{v}|^2 (\vec{v}\cdot\vec{n})\, dS\right) \quad . \tag{4}$$

The advective term includes the spatial acceleration and the kinetic term include the temporal acceleration. As with the Unsteady Bernoulli (streamline) approach [20], gravity and viscosity is assumed to have no significant impact on the resulting pressure difference.

III. Material and Methods

This section presents the ultrasound sequence, the velocity estimation, and the equipment used for the phantom study.

A. Sequence

An interleaved SAU sequence with 12 virtual sources is used for flow imaging [23]. It employs 32 active elements in transmit and 128 multiplexed elements in receive. The correlation frames are only separated by the pulse repetition time, making the interleaved sequence ideal for detecting high velocities [24].

B. Velocity estimation

The experiment was performed on a blood vessel using a linear array probe. The linear array probe was restricted by its geometry to only capture the in-plane motion. The out-of-plane motion is, thus, not included. Furthermore, the work energy method requires blood velocity information in cross-sections and it is therefore necessary to assume rotational symmetric blood vessels. This can be seen in Fig. 1, which gives an illustrative overview of how the velocity data are used. The inlet and outlet velocities are calculated using vector flow guided directional cross-correlation. Here, vector flow imaging (VFI) [25] is used to estimate the direction of flow and cross-correlation [26] [27] is used to estimate the velocity along that direction. To increase the frame rate, recursive imaging [28] is applied as described in [20]. The resulting velocity profiles are then used for calculating the flow rate in (2) and the advective energy rate in (4). The kinetic energy term (3) requires velocities inside a volume defined by the inlet plane and the outlet plane. Here directional cross-correlation would be too computational demanding and to save time, VFI-velocities are used as $\vec{v}$.

C. Material

Data are acquired with a GE-L3-12D, 5.2 MHz linear transducer (GE Healthcare, Chicago, Illinois, USA) connected to a Vantage 256 research scanner (Verasonics, Kirkland, Washington, USA) with a pulse repetition frequency of 5 kHz. The virtual sources are evenly distributed across the entire aperture width. The experiment is performed on a tissue mimicking blood vessel phantom and is connected to a pulsating flow pump (CompuFlow 1000, Shelly, Medical Imaging Technologies, Toronto, Canada). It applies a volume profile that mimicks the carotid artery with a peak flow rate of 12.9 mL/s and an average flow rate of 3.9 mL/s.

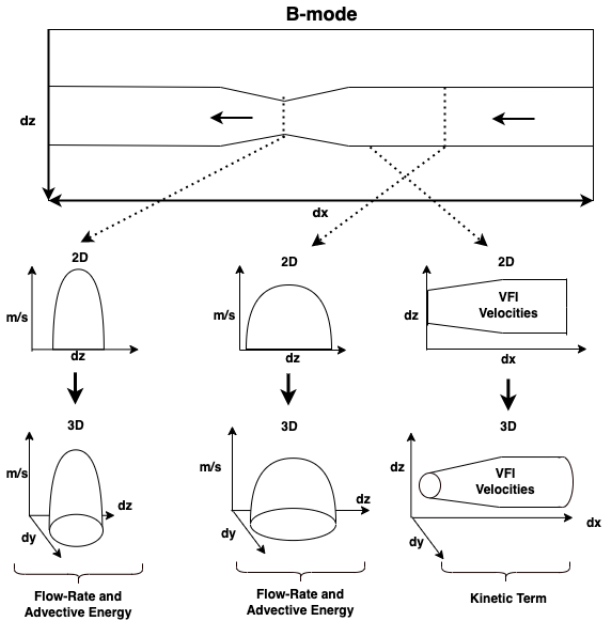

Fig. 1: Shows how the 2D cross-sectional profiles are used for constructing the 3D profiles. The parabolic velocity profiles are calculated based on the directional cross-correlation method and are used for the surface integrals in (4) and (2). The VFI velocity is used in the Kinetic energy term (3).

IV. Experimental Result

This section describes the results obtained from the two methods when applied to experimental data. Fig. 2 shows two B-mode images of the same blood vessel. The top image shows the selected streamline used for the unsteady Bernoulli method and the bottom image shows the inlet and the outlet plane used for the work-energy method. The flow is going from right to left in the images. Fig. 3 shows the estimated flow rate used

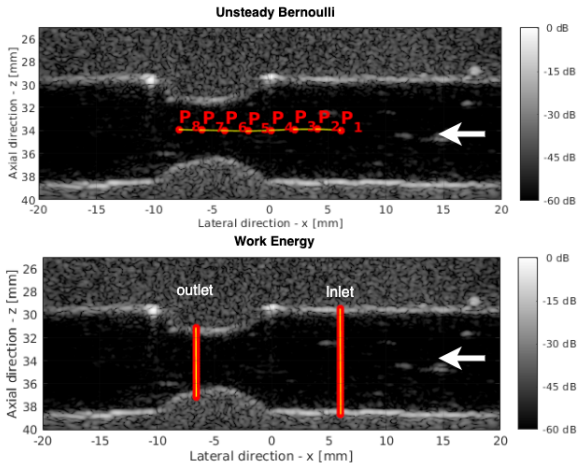

Fig. 2: Top image shows the position of the streamline and the bottom image shows the position of the inlet and outlet planes used by the work energy method. The pressure differences are then estimated between p8 and p1, and between outlet and inlet.

in the work energy method along with the average flow rate (dashed line) at the inlet and at the outlet. Both are estimated using (2). The peak flow-rate is estimated through the inlet

and the outlet, and is estimated to be 6.64 mL/s and 6.70 mL/s. The average flow rate is estimated to be 3.06 mL/s and 2.97 mL/s for the inlet and outlet, respectively. Fig. 4 shows

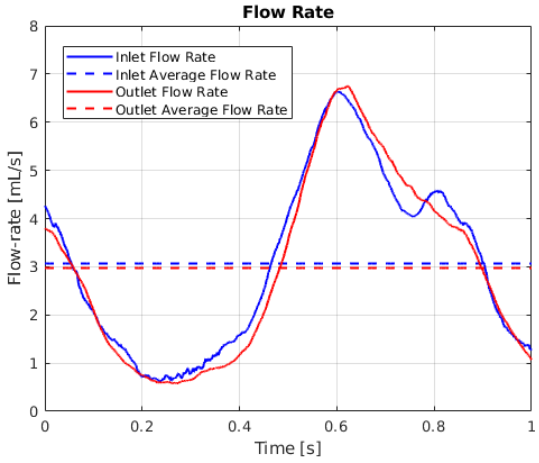

Fig. 3: Shows the flow rate at the inlet and at the outlet for 1 s of data. The peak flow rate for the inlet and outlet are 6.64 mL/s and 6.70 mL/s. The average flow rate are 3.06 mL/s and 2.97 mL/s.

the pressure difference from the advective term (Orange) and the kinetic term (Yellow) along with the combined pressure difference for a single flow cycle (Blue). It is seen that the advective pressure difference is the largest contributor to the total pressure difference. Fig. 5 compares the pressure gradient

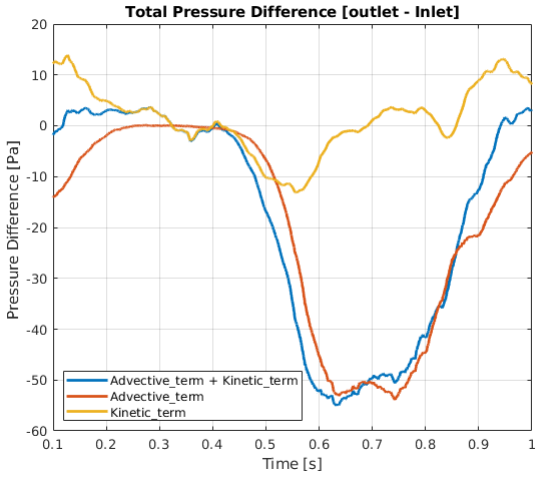

Fig. 4: Shows the pressure difference between the outlet and the inlet. The yellow curve represents the kinetic term and the red curve represents the advective term. The blue curve shows the total pressure difference, when combining the kinetic and advective term.

from the two methods and shows the mean pressure difference. The grey area denotes $\pm$ one standard deviation. The work energy method (blue-line) estimates pressure difference in the range between 3.42 Pa and -53.3 Pa with a coefficient of variation of 3.04%. The unsteady Bernoulli method (red-line) estimates pressure differences in the range between 5.44 Pa and -68.2 Pa with a coefficient of variation of 3.23%. This is based on eleven flow cycles aligned in time, with one flow cycle excluded due to air bubbles (The pump setup is not free from air bubbles). If this flow cycle is included, the new method remains robust (Coefficient of variation = 3%), compared to the unsteady Bernoulli method (Coefficient of variation = 4.17%).

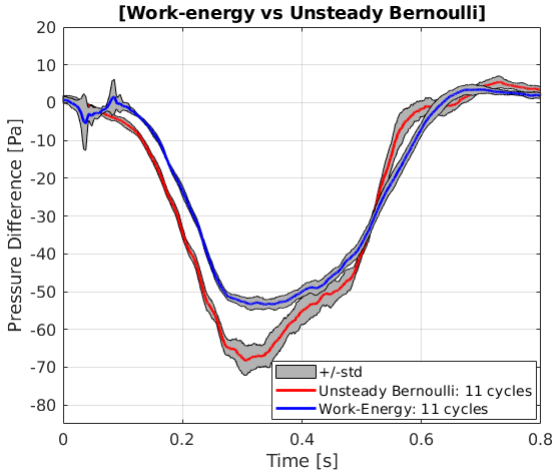

Fig. 5: Compares the pressure gradient from the work energy method (blue-line) to the unsteady Bernoulli method (red-line).

V. Discussion

The peak flow rate is set to 12.9 mL/s and has an average flow rate of 3.9 mL/s. Since the phantom is connected by tubes the measured peak flow rate is expected to be lower than what is set by the pump. However, the average flow rate is expected to remain the same. The results in Fig. 3 shows that the average flow rate is 3.06 mL/s and 2.97 mL/s for the inlet and for the outlet. This is lower than the expected average flow rate of 3.9 mL/s. One explanation could be that the phantom blood vessel is not entirely rotational symmetric when being scanned. Even small pressure exerted by the probe may cause the blood vessel to become more elliptic than circular and thus challenge the assumption of rotational symmetry, leading to an underestimation of the flow rate. Another explanation is that the phantom is made of tissue mimicking materials, which stretch and expand during pulsatile flow. This can also influence the measured flow rate.

This study used a clinically available linear probe. Since the method requires velocities in cross-sections, it is necessary to assume that the blood vessel is rotational symmetric. This allows cross-sections of velocities to be modelled from in-plane velocities captured by the probe. This also means that the method only applies to blood vessels with a symmetric stenosis, which is not always the case. Another source of error is when a symmetric blood vessel experiences a non-symmetric flow. This can happen after a bifurcation, where the blood flow can be skewed towards a small section of the inner wall as shown in [29]. Here, the reconstruction algorithm will assume rotational symmetry even though the velocities are confined to a small region captured by the transducer. This will cause an overestimation of the flow flux and thus wrong pressure gradients. A solution to these problems is to apply 3D ultrasound imaging with high volume rates [30]. This would allow velocities to be captured in all three planes.

VI. Conclusion

The work energy method detected smaller pressure differences ranging from 3.42 Pa to -53.3 Pa compared to the unsteady Bernoulli method, which detected pressure differences ranging from 5.44 Pa to -68.2 Pa. The precision of the two methods was estimated across 11 flow cycles and showed a slight improvement to the work energy method. It detected a coefficient of variation of 3.04% compared to the unsteady Bernoulli method, which detected a coefficient of variation of 3.23%. This was measured using a clinical available probe, which necessitates rotational symmetric blood vessels.

VII. Acknowledgement

The work is supported by the ERC Synergy Grant: SURE-3-D Super resolution Ultrasound Real time imaging of Erythrocytes, grant number: 854796.

References

[1] A. Vahanian, F. Beyersdorf, F. Praz, M. Milojevic, S. Baldus, J. Bauersachs, D. Capodanno, L. Conradi, M. D. Bonis, R. D. Paulis *et al.*, "2021 ESC/EACTS guidelines for the management of valvular heart disease: Developed by the task force for the management of valvular heart disease of the european society of cardiology and the european association for cardio-thoracic surgery," *EACTS*, vol. 60, no. 4, pp. 727–800, 2021.

[2] R. A. Nishimura and B. A. Carabello, "Hemodynamics in the cardiac catheterization laboratory of the 21st century," *Circulation*, vol. 125, no. 17, pp. 2138–2150, 2012.

[3] J. Holen, R. Aaslid, and K. Landmark, "Determination of pressure gradient in mitral stenosis with a non-invasive ultrasound Doppler technique," *Acta med. scand.*, vol. 32, pp. 455–460, 1976.

[4] L. Hatle, A. Brubakk, A. Tromsdal, and B. Angelsen, "Noninvasive assessment of the pressure drop in mitral stenosis by Doppler ultrasound," *British Heart J.*, pp. 131–140, 1978.

[5] R. Yotti, J. Bermejo, J. C. Antoranz, M. M. Desco, C. Cortina, J. L. R. Alvarez, C. Allue, L. Martin, M. Moreno, J. A. Serrano, R. Munoz, and M. A. G. Fernandez, "A noninvasive method for assessing impaired diastolic suction in patients with dilated cardiomyopathyc," *Circulation*, vol. 112, no. 19, pp. 2921–2929, 2005.

[6] R. Yotti, J. Bermejo, J. C. Antoranz, J. L. Rojo-Alvarez, C. Allue, J. Silva, M. M. Desco, M. Moreno, and M. A. Garcia-Fernandez, "Noninvasive assessment of ejection intraventricular pressure gradients," *J. Am. Coll. Cardiol.*, vol. 43, no. 9, pp. 1654–1662, 2004.

[7] M. S. Firstenberg, P. M. Vandervoort, N. L. Greenberg, N. G. Smedira, P. M. McCarthy, M. J. Garcia, and J. D. Thomas, "Noninvasive estimation of transmitral pressure drop across the normal mitral valve in humans: Importance of convective and inertial forces during left ventricular filling," *J. Am. Coll. Cardiol.*, vol. 36, no. 6, pp. 1942–1949, 2000.

[8] J. B. Olesen, C. A. Villagómez Hoyos, N. D. Møller, C. Ewertsen, K. L. Hansen, M. B. Nielsen, B. Bech, L. Lönn, M. S. Traberg, and J. A. Jensen, "Non-invasive estimation of pressure changes using 2-D vector velocity ultrasound: An experimental study with in-vivo examples," *IEEE Trans. Ultrason. Ferroelec. Freq. Contr.*, vol. 65, no. 5, pp. 709–719, 2018.

[9] C. A. Villagomez-Hoyos, M. B. Stuart, K. L. Hansen, M. B. Nielsen, and J. A. Jensen, "Accurate angle estimator for high frame rate 2-D vector flow imaging," *IEEE Trans. Ultrason. Ferroelec. Freq. Contr.*, vol. 63, no. 6, pp. 842–853, 2016.

[10] M. O'Donnell and L. J. Thomas, "Efficient synthetic aperture imaging from a circular aperture with possible application to catheter-based imaging," *IEEE Trans. Ultrason. Ferroelec. Freq. Contr.*, vol. 39, pp. 366–380, 1992.

[11] J. A. Jensen and S. I. Nikolov, "Directional synthetic aperture flow imaging," *IEEE Trans. Ultrason. Ferroelec. Freq. Contr.*, vol. 51, no. 9, pp. 1107–1118, 2004.

[12] ——, "Transverse flow imaging using synthetic aperture directional beamforming," in *Proc. IEEE Ultrason. Symp.*, 2002, pp. 1488–1492.

[13] P. J. Kilner, G. Z. Yang, R. H. Mohiaddin, D. N. Firmin, and D. B. Longmore, "Helical and retrograde secondary flow patterns in the aortic arch studied by three-directional magnetic resonance velocity mapping," *Circulation*, vol. 88, no. 5, pp. 2235–2247, 1993.

[14] S. B. S. Krittian, P. Lamata, C. Michler, D. A. Nordsletten, J. Bock, C. P. Bradley, A. Pitcher, P. J. Kilner, M. Markl, and N. P. Smith, "A finite-element approach to the direct computation of relative cardiovascular pressure from time-resolved MR velocity data," *Medical image analysis*, vol. 16, no. 5, pp. 1029–1037, 2012.

[15] H. Svihlova, J. Hron, J. Malek, K. Rajagopal, and K. Rajagopal, "Determination of pressure data from velocity data with a view toward its application in cardiovascular mechanics. part 1. Theoretical considerations," *Int. J. Eng. Sci.*, vol. 105, pp. 108–127, 2016.

[16] F. Donati, C. A. Figueroa, N. P. Smith, P. Lamata, and D. A. Nordsletten, "Non-invasive pressure difference estimation from PC-MRI using the work-energy equation," *Med. Image Anal.*, vol. 26, pp. 159–172, 2015.

[17] D. Marlevi, B. Ruijsink, M. Balmus, D. Dillon-Murphy, D. Fovargue, K. Pushparajah, C. Bertoglio, M. Colarieti-Tosti, M. Larsson, P. Lamata, C. A. Figueroa, R. Razavi, and D. A. Nordsletten, "Estimation of cardiovascular relative pressure using virtual work-energy," *Nature*, vol. 9, no. 1, pp. 1375–1391, 2019.

[18] D. Marlevi, H. Ha, D. Dillon-Murphy, J. F. Fernandes, D. Fovargue, M. Colarieti-Tosti, M. Larsson, P. Lamata, C. A. Figueroa, T. Ebbers, and D. A. Nordsletten, "Non-invasive estimation of relative pressure in turbulent flow using virtual work-energy," *Med. Image Anal.*, vol. 60, p. 101627, 2020.

[19] D. Marlevi, M. Balmus, A. Hessenthaler, F. Viola, D. Fovargue, A. de Vecchi, P. Lamata, N. S. Burris, F. D. Pagani, J. Engvall, E. R. Edelman, T. Ebbers, and D. A. Nordsletten, "Non-invasive estimation of relative pressure for intracardiac flows using virtual work-energy," *Med. Image Anal.*, vol. 68, 2021.

[20] L. E. Haslund, L. T. Jørgensen, M. S. Traberg, M. B. Stuart, and J. A. Jensen, "Precise estimation of intravascular pressure gradients," *IEEE Trans. Ultrason. Ferroelec. Freq. Contr.*, vol. 70, no. 5, pp. 393–405, May 2023.

[21] C. M. Porth, *Essentials of Pathophysiology*. Wolters Kluwer, 2015.

[22] F. Donati, S. Myerson, M. M. Bissell, N. P. Smith, S. Neubauer, M. J. Monaghan, D. A. Nordsletten, and P. Lamata, "Beyond Bernoulli - Improving the accuracy and precision of noninvasive estimation of peak pressure drops," *Circ Cardiovasc Imaging*, pp. 1–9, 2017.

[23] J. A. Jensen, B. G. Tomov, L. E. Haslund, N. S. Panduro, and C. M. Sørensen, "Universal synthetic aperture sequence for anatomic, functional and super resolution imaging," *IEEE Trans. Ultrason. Ferroelec. Freq. Contr.*, vol. 70, no. 7, pp. 708–720, 2023.

[24] J. A. Jensen, "Estimation of high velocities in synthetic aperture imaging: I: Theory," *IEEE Trans. Ultrason. Ferroelec. Freq. Contr.*, vol. 66, no. 6, pp. 1024–1031, 2019.

[25] ——, "Directional transverse oscillation vector flow estimation," *IEEE Trans. Ultrason. Ferroelec. Freq. Contr.*, vol. 64, no. 8, pp. 1194–1204, 2017.

[26] S. I. Nikolov and J. A. Jensen, "In-vivo synthetic aperture flow imaging in medical ultrasound," *IEEE Trans. Ultrason. Ferroelec. Freq. Contr.*, vol. 50, no. 7, pp. 848–856, 2003.

[27] J. Kortbek and J. A. Jensen, "Estimation of velocity vector angles using the directional cross-correlation method," *IEEE Trans. Ultrason. Ferroelec. Freq. Contr.*, vol. 53, pp. 2036–2049, 2006.

[28] S. I. Nikolov, K. Gammelmark, and J. A. Jensen, "Recursive ultrasound imaging," in *Proc. IEEE Ultrason. Symp.*, vol. 2, 1999, pp. 1621–1625.

[29] M. Motomiya and T. Karino, "Flow patterns in the human carotid artery bifurcation," *Stroke*, vol. 15, no. 1, pp. 50–56, 1984.

[30] L. T. Jørgensen, M. S. Traberg, M. B. Stuart, and J. A. Jensen, "Performance assessment of row-column transverse oscillation tensor velocity imaging using computational fluid dynamics simulation of carotid bifurcation flow," *IEEE Trans. Ultrason. Ferroelec. Freq. Contr.*, vol. 69, no. 4, pp. 1230–1242, 2022.